IEEJ TRANSACTIONS ON ELECTRICAL AND ELECTRONIC ENGINEERING
IEEJ Trans 2011; **6**: 180–189
Published online in Wiley Online Library (wileyonlinelibrary.com). DOI:10.1002/tee.20642

Paper

Multiphysics Analysis for Micro Electromechanical Systems Based on Electrical Circuit Simulator

Makoto Mita[*,**], Member
Satoshi Maruyama[**,***], Student Member
Yuheon Yi[**,***], Non-member
Kazuhiro Takahashi[**,****], Member
Hiroyuki Fujita[**], Member
Hiroshi Toshiyoshi[**,*****a], Member

We report a newly developed equivalent electrical circuit for microelectromechanical systems (MEMS) based on a circuit simulator Qucs (Quite Universal Circuit Simulator). An analog computing solver for the equation of motion (EOM) has been interpreted to an electrical equivalent circuit by using an electrical capacitor as an ideal mathematic integrator. Viscoelastic suspension and electrostatic parallel-plate actuator are modeled as equivalent subcircuits that can be cosolved with the EOM module. Those subcircuit models are used as building blocks to numerically simulate the behavior of various types of MEMS actuators. Thanks to the well-prepared simulation toolbox of Qucs, multiphysics analysis of micromechanical and electrical quantities has become straightforward on a single platform. Equivalent circuit models for coupled oscillator and parallel-plate electrostatic actuator (including mechanical contact after electrostatic pull-in) are presented as a verification program to examine the simulation accuracy. © 2011 Institute of Electrical Engineers of Japan. Published by John Wiley & Sons, Inc.

Keywords: multiphysics simulation, behavior model, macro model, equivalent circuit

Received 25 January 2010; Revised 16 April 2010

1. Introduction

Various types of behavioral simulation tools for microelectromechanical systems (MEMS) have been developed to deal with multiphysics phenomena since the early stage of MEMS [1–5]. The electrostatic micro actuator is a good target for MEMS cosolvers which process the iteration of elastic and electrostatic analysis until the electrostatic force finds an equilibrium solution with the elastic restoring force. Along with the development of diverging MEMS applications, multiphysics simulation has been extended to various disciplines such as fluidics, optics, microwave electronics, and, of course, microelectronics.

The significance of multiphysics simulators is acknowledged in the field of integrated MEMS. A microelectromechanical device alone cannot deliver an added value to a MEMS product today but a microelectromechanical 'system' as a whole has to be designed to meet with the specification and cost. It is thus becoming a straightforward approach to designing microelectromechanical components in a top-down manner to satisfy the system requirements, rather than tuning the entire MEM system for a microelectromechanical component developed in a bottom-up manner. The electrostatic silicon resonator is a good example; the resonant frequency is not a sole design parameter but the electrostatic bias voltage must be consistent with the operation voltage of the peripheral electrical components [6]. Electromechanical behavior of such MEMS should be designed and verified at the system simulation level before stepping down to device engineering. Similarity in electromechanical integration can also be found in other applications such as CMOS-MEMS accelerometer [7], digital micromirror device [8], and silicon microphone [9].

Commercial MEMS simulation tools are becoming powerful by acquiring optional toolboxes for various types of MEMS applications. Some software can handle multiphysics simulation on both micromechanical components and electrical circuits [10,11]. Besides the cost of such commercial software, a drawback is that the device models and simulation algorithms are a black box to users, and hence we experience difficulty in building a simulation model for our own device that is not commonly supported in the standard component library of commercial MEMS simulators. For this reason, we have used electrical circuit simulation software Qucs (Quite Universal Circuit Simulator) for the first time to implement a multiphysics equivalent circuit model for electrostatic microactuators [12,13]. Qucs is open-source software subject to the general public license (GPL) agreement, and users have free access to the device models and the source codes. It is also an agile tool to develop subcircuit modules for MEM actuators and sensors that can be inserted into the electrical circuit simulation models. The seamless interface between micromechanics and electronics enables us to perform multiphysics simulation in a straightforward manner on a single simulation platform.

In this paper, we present equivalent circuit models for MEMS electrostatic actuators, in order to provide the readers with the

[a] Correspondence to: Hiroshi Toshiyoshi. E-mail: hiro@iis.u-tokyo.ac.jp

* Institute of Space and Astronautical Science, Japan Aerospace Exploration Agency, 3-1-1 Yoshinodai, Sagamihara, Kanagawa 229-8510, Japan

** Institute of Industrial Science, The University of Tokyo, 4-6-1 Komaba, Meguro-ku, Tokyo 153-8505, Japan

*** Department of Electrical Engineering and Information Systems, Graduate School of Engineering, The University of Tokyo, 7-3-1 Hongo, Bunkyo-ku, Tokyo 113-8654, Japan

**** Currently with Toyohashi University of Technology, 1-1 Hibarigaoka, Tenpaku-cho, Toyohashi, Aichi 441-8580, Japan

***** Research Center for Advanced Science and Technology, The University of Tokyo, 4-6-1 Komaba, Meguro-ku, Tokyo 153-8904, Japan

skill to develop their own simulation toolbox. For the simplicity of device model construction, we did not use the electromechanical analogy but developed an equivalent electrical circuit model for the equation of motion (EOM). Verification problems are also presented to test the simulation reproducibility of frequency response analysis and nonlinear transient analysis including electrostatic pull-in.

2. Equivalent Circuit Models for MEMS Actuator

2.1. Analytical model for electrostatic actuator

Figure 1 illustrates an analytical model for a parallel-plate electrostatic actuator. A plate of area S and mass m is suspended with a spring of elastic constant k and with a dashpot of damping coefficient c. The movable plate is biased to V_A (ground level, $V_A = 0$, in Fig. 1), and the mechanically fixed plate at the bottom is electrically biased to voltage V_B through an electrical resistance R. The following equations are used to describe the electromechanically coupled motion x of the movable plate. First, the electrostatic force is

$$F_E = \frac{1}{2}\varepsilon_0 \frac{S}{(g-x)^2}(V_B - V_A)^2 \tag{1}$$

where $\varepsilon_0 = 8.854 \times 10^{-12}$ F/m is the dielectric constant of vacuum (air), and g is the initial gap length between the plates [14]. In (1), we ignore the fringe effect of the electrical field on the plate edges. Upon the drive voltage application, surface charge is induced as

$$Q_A = \varepsilon_0 \frac{S}{g-x}(V_A - V_B) \tag{2}$$

and

$$Q_B = \varepsilon_0 \frac{S}{g-x}(V_B - V_A) \tag{3}$$

on the top and bottom electrodes, respectively. The charge induction automatically causes the electromechanical coupling between the actuator and the driver circuit, and hence the user does not have to explicitly describe an equation coupling the electromechanical behavior of the actuator and the electrical circuit. Due to the electrical current flowing through the resistance R, the voltage measured at the plate V_B becomes lower than the external drive voltage V, i.e.

$$V_B = V - R \cdot i \tag{4}$$

where the charge/discharge current i is expressed as

$$i = \frac{d}{dt}[C \cdot (V_B - V_A)] \tag{5}$$

In this form, we presume that the electrostatic capacitance $C = \varepsilon_0 S/(g-x)$ varies as a function of time due to the plate motion $x(t)$. Finally, the overall oscillation system is governed by the EOM:

$$m\ddot{x} + c \cdot \dot{x} + k \cdot x = F_E \tag{6}$$

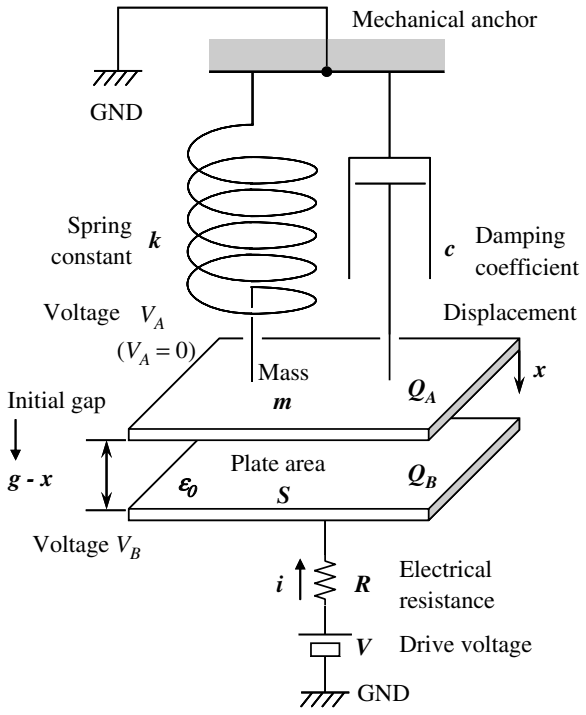

Fig. 1. Analytical model for parallel-plate electrostatic micro actuator

2.2. Equivalent circuit model for integral equation

In a typical system simulation model such as MATLAB/Simulink [11], the EOM (6) is rewritten in the form of acceleration as follows:

$$\ddot{x} = (F_E - c \cdot \dot{x} - k \cdot x)\frac{1}{m} \tag{7}$$

and the differential equation is solved in a block diagram as shown in Fig. 2. Velocity $\dot{x}$ and position x are numerically computed through a series of integration (Laplace transform, $1/s$), and the values are passed backward through the feedback loops to find a consistent value for $\ddot{x}$. This approach is convenient to comprehend the behavior of a linear system from a control theory point of view but one may need to use a conversion tool to insert an electrical circuit model into the simulation block diagram [10,15,16].

We used electrical capacitance as an ideal mathematic integrator that stores incoming electrical current and returns the result as a built-up voltage, i.e.

$$V = \frac{1}{C}\int_0^\tau i dt \tag{8}$$

Use of an electrical capacitance as an integrator has long been known in the field of analog computing and also in MEMS simulation [17,18]. Analog computing using electrical circuitry has been replaced with digital computation today due to the insufficient simulation accuracy associated from the stray capacitance and current leakage of actually implemented analog circuits. Nevertheless, the idea of using a capacitance is still effective in the computer-based simulation, which is free from stray capacitance or leakage. As shown in Fig. 3, we simply used a capacitor as a mathematic integrator by reading the input electrical current as acceleration $\ddot{x}$, and the output voltage as velocity $\dot{x}$. In (8), the capacitance value C

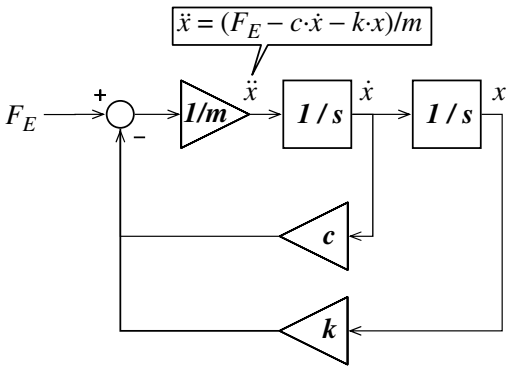

Fig. 2. Typical solving block diagram for the equation of motion

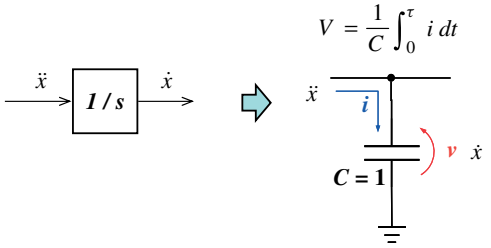

Fig. 3. Electrical circuit implementation of mathematic integral using an ideal electrical capacitor

is set to be 1 F in order to have unity gain for the dimensionless electrical operation of $\dot{x} = \int_0^\tau \ddot{x}dt$. The same procedure is used to integrate velocity $\dot{x}$ to obtain position x.

2.3. Equivalent circuit model for parallel-plate actuator Figure 4 is an equivalent circuit model for a parallel-plate electrostatic microactuator [13]. Among the many circuit simulators, we chose open-source freeware Qucs on Windows PC as an operation platform, due to a particular reason that it is highly versatile in electrical component programming called equation defined device (EDD). EDD is a programmable current source of Qucs, and its $I-V$ characteristics can be described by using an algebraic equation.

EDD_1 in Fig. 4 is made up of four current sources that are cross-referenced to each other to define a current output as a function of input voltages. In this case, the first current source in EDD_1 represents the electrostatic force (1) as a constant current

$$I_1 \leftarrow (1/2)^*\mathrm{ep}_0^*S^*(V_3 - V_2)\hat{}2/(g - V_4)\hat{}2 \tag{9}$$

where V_2, V_3, and V_4 are Qucs translation of V_A, V_B, and x, respectively. The constant parameters ep_0, S, and g are the dielectric permittivity ε_0, the plate area, and the initial gap between the plates, respectively. Note that variables written in block letters are equations in the EDD property box and that the arrow (←) represents substitution, while those in italic letters are for mathematic description of the models. Symbols *, /, and ^ are the native notations of Qucs EDD representing mathematic multiplication, division, and power operations, respectively. The variables used in the EDD expressions are regarded as dimensionless, and those expressed in voltage or current can be read in any units (such as m, m/s, or m/s; [2]) in an *ad hoc* manner. More than 100 algebraic operations and mathematic functions are available for the EDD expressions; it enables us to describe various sorts of MEMS devices so long as we know an equation to model with; for instance, optical ray tracing can also be implemented by the EDD function to develop a complete model for an MEMS optical scanner reported elsewhere [19]. The EDD function in Qucs corresponds to the nonlinear dependent source function of Simulation Program with Integrated Circuit Emphasis (SPICE), and hence the approach developed in this work can also be implemented in SPICE.

Qucs EDD is designed to accept only voltage as input and to generate current as output. Therefore, a current-controlled voltage source (CCVS) is used to convert the electrostatic force 'current' from EDD_1 into a force 'voltage' at a conversion rate of unity, before passing to EDD_2. EDD_2 in Fig. 4 is the EOM solver, which is defined after (7) as

$$I_1 \leftarrow (V_2 - c^*V_3 - k^*V_4)/m \tag{10}$$

where V_2, V_3, and V_4 correspond to force F, velocity $\dot{x}$, and position x, respectively. The constant parameters m, c, and k are passed to the EDD as an argument.

In this work, mathematic integration is electrically interpreted by using capacitor C_1 that stores the electrical current signal of $\ddot{x}$ and returns a voltage signal of $\dot{x}$. Another integration step from velocity $\dot{x}$ to position x is processed in the same manner by using C_2. Both capacitor values are set to be 1 F; they seem to be excessive for a realistic value of an electronic component but Qucs simply processes it as a numeral without causing computation errors. A voltage-controlled current source (VCCS) is inserted between C_1 and C_2 to decouple the two integration steps; without the VCCS, capacitors C_1 and C_2 make a single-step integration. Another

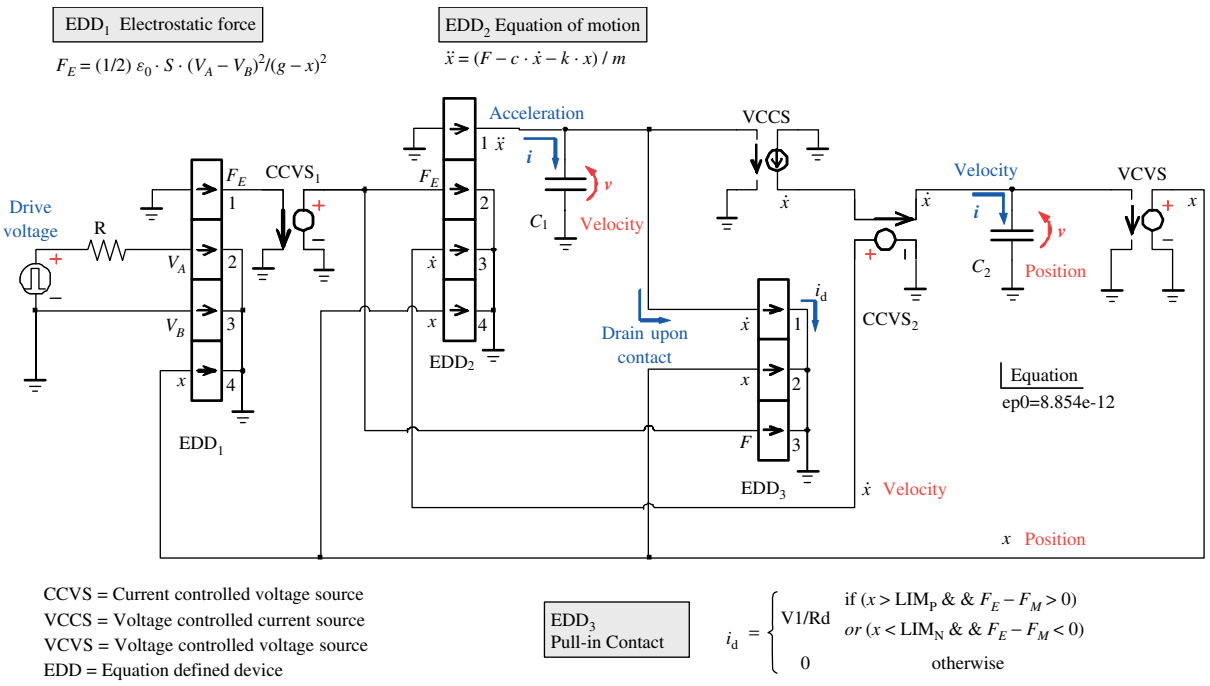

Fig. 4. Equivalent circuit model for the overall parallel-plate electrostatic micro actuator including the equation of motion. Three EDD blocks are used to implement electrostatic attractive force (EDD_1), acceleration (EDD_2), and pull-in contact subroutine (EDD_3). Velocity and displacement are calculated from the acceleration through the series of electrical integrations using capacitors C_1 and C_2

CCVS before C_2 is to monitor the current signal of $\dot{x}$ and to make the voltage signal $\dot{x}$. Integration result of C_2 is also read as voltage by using a voltage-controlled voltage source (VCVS) of unity conversion factor. The voltage signals of $\dot{x}$ and x are passed backward to EDD_1 and EDD_2, where they are referenced to numerically calculate the electrostatic force F_E and acceleration $\ddot{x}$, respectively.

2.4. Electrostatic pull-in and release EDD_3 in Fig. 4 is an auxiliary path to handle the electrostatic pull-in condition, at which the movable plate spontaneously trips to the counter electrode due to the electrostatic attractive force that exceeds the mechanical restoring force. Mechanical stoppers are usually used to limit the displacement and to avoid electrical short circuit upon full contact. Electrostatic pull-in is beneficial to latch the movable plate with low voltage and to digitize the actuator's motion [20,21]. The pull-in mechanism can also be used to make a self-oscillating MEMS device such as a random number generator and a voltage-controlled oscillator [22,23]. Despite the usefulness of the pull-in phenomenon, it is usually disregarded in multiphysics analysis of MEMS because of the difficulty in converting the nonlinear terms into the net-list expression [24–27].

EDD of Qucs can handle conditional branch using an if-clause in the equation, and we used it to judge the mechanical contact of the movable plate. Upon pull-in contact, the motion is stopped and thus the velocity $\dot{x}$ is forced to be zero. This phenomenon is interpreted in the equivalent circuit by discharging the integral capacitor C_1 to zero through EDD_3. If we set the displacement limiters at LIM_P and LIM_N on the positive and negative directions, respectively, the discharge current I_1 of EDD_3 is programmed as

$$I_1 \leftarrow \underbrace{(V_2 >= \mathrm{LIM_P} \,\&\&\, V_3 - k^{*}V_2 >= 0) \,\|\, (V_2 >= \mathrm{LIM_N} \,\&\&\, V_3 - k^{*}V_2 <= 0)?}_{\text{if-clause}} \quad \underbrace{V_1/\mathrm{R_d}}_{\text{then-clause}} : \underbrace{0}_{\text{else-clause}} \tag{11}$$

where the Qucs symbols && and || represent logical AND and OR operations, respectively. When the movable plate is out of the pull-in range, there is no discharge path formed, and C_1 works as a linear integrator. When the movable plate trips to the stopper position on the positive side ($V_2 >= \mathrm{LIM_P}$), on the other hand, capacitor C_1 is forced to discharge at a rate of $I_1 = V_1/\mathrm{Rd}$ until emptied so long as the electrostatic force remains to be greater than the mechanical restoring force ($V_3 - k * V_2 >= 0$). A similar description has been made for the negative side stopper. Once the plate falls into the pull-in position, the if-clause is valid until the electrostatic force becomes smaller than the mechanical restoring force; at this moment, the plate is released to the rest position. Note that a single column of EDD_3 can handle both electrostatic pull-in and release conditions.

The coefficient R_d is an artificially introduced factor called a 'drain resistance' in this pull-in subroutine, and it corresponds to a virtual electrical resistance for discharging C_1. Due to the drain current being proportionally regulated by V_1, capacitor C_1 is swiftly discharged to zero but not overly discharged. The appropriate values for R_d have been empirically found to be smaller than 10^{-14} for a typical MEMS actuator. Electromechanical interpretation for R_d is discussed later in Section 4.3.

3. Subcircuit Models for MEMS Elements

3.1. Equation of motion solver Three primary components (EOM, electrostatic actuator, and suspensions) are flattened in the equivalent circuit model discussed in the previous section, and one may need to modify the wiring or parameters every time it is adapted to a new actuator design. For a larger scale integration MEMS, flattened circuits occupy a large area on the PC screen and it becomes difficult to look over. For these reasons, we have modified the Qucs model into subcircuits with the standardized input and output (I/O) connections; it has attained versatility as a building block for a wide range of microelectromechanical devices.

The kernel component is the solver for the EOM, which is designed to deliver the calculated displacement x and velocity $\dot{x}$ as a function of applied external force. Figure 5(a) is a subcircuit symbol of the EOM solver. The I/O pins are arranged on both left- and right-hand sides of the subcircuit symbol so that other components such as spring and actuator can be connected in a

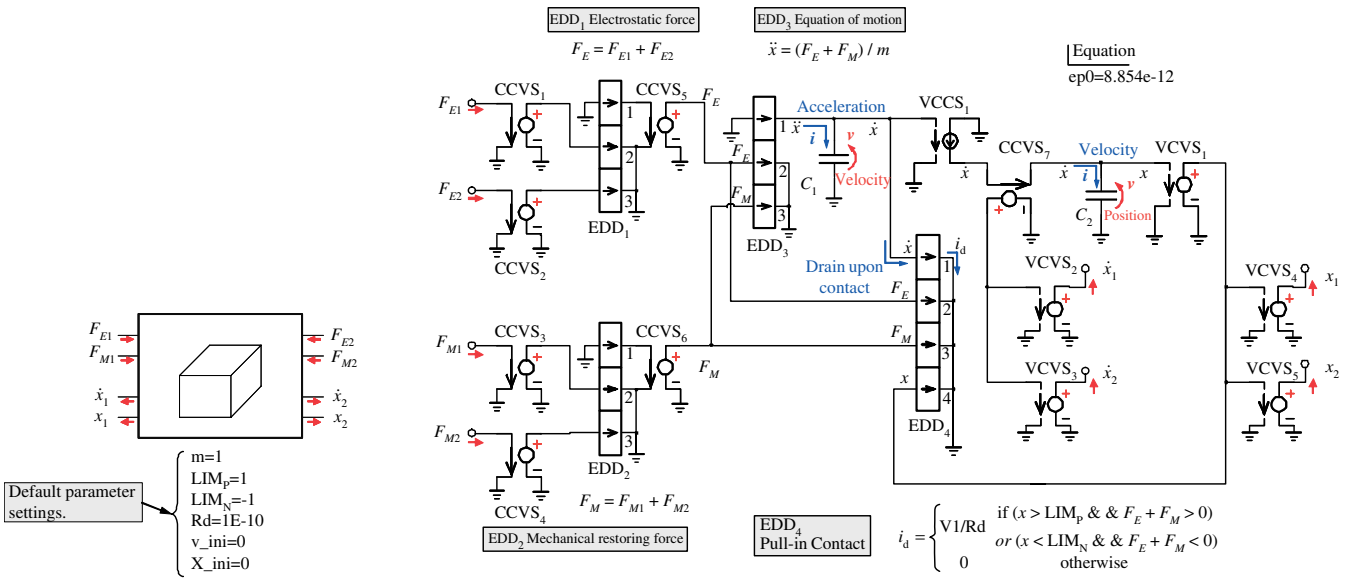

Fig. 5. Generalized subcircuit model for the equation of motion solver: (a) circuit symbol and (b) subcircuit model. Each of incoming electrostatic forces and mechanical restoring forces on the both sides of the module are first added into one by EDD_1 and EDD_2. Acceleration is calculated in EDD_3, after which velocity and displacement are generated by the series of electrical integration using two capacitors C_1 and C_2, and returned from the output ports $VCVS_2$ to $VCVS_5$

straight chain. The electrostatic force and the mechanical restoring force have separate input pins at the interface, and their magnitudes are compared within the EOM subcircuit to judge the electrostatic pull-in condition.

We use an inertia system to coordinate the force and displacement to be positive in the $+X$ direction in each element. In the EOM diagram shown in Fig. 5(b), EDD_1 adds the incoming pair of electrostatic forces, namely F_{E1} and F_{E2}, acting on both sides of the module, and calculates the net electrostatic force $F_E = F_{E1} + F_{E2}$ by the EDD_1 equation $I_1 \leftarrow V_2 + V_3$, where V_2 and V_3 represent F_{E1} and F_{E2}, respectively. EDD_2 does the same operation to the elastic restoring forces: $F_M = F_{M1} + F_{M2}$. The EOM has been designed to have duplicated I/O ports on both sides for the convenience of connecting a suspension and an actuator unit in a straight chain and to help users comprehend the correspondence between the actual device and the simulation model. EDD_3 has been copied and modified from EDD_2 in Fig. 4; the incoming electrostatic and mechanical forces are merged and divided by the mass m to calculate the acceleration as $\ddot{x} = (F_E + F_M)/m$. EDD_4 corresponds to EDD_3 in Fig. 4, and it handles the electrostatic pull-in. According to the separation of the net electrostatic force and the net mechanical force, the conditioning equation (12) has been modified to

$$I_1 \leftarrow \underbrace{\begin{array}{l}(V_4 >= \mathrm{LIM_P} \;\&\&\; V_2 + V_3 >= 0) \| \\ (V_4 <= \mathrm{LIM_N} \;\&\&\; V_2 + V_3 <= 0)?\end{array}}_{\text{if-clause}} \underbrace{V_1/\mathrm{R_d}}_{\text{then-clause}} : \underbrace{0}_{\text{else-clause}}, \tag{12}$$

where (V_2, V_3, V_4) is $(F_E,\ F_M,\ x)$. This subroutine is not limited to the electrostatic pull-in but also can be generally applied to mechanical displacement limiters. Although the actual pull-in behavior takes place in the electrostatic actuator unit, we included the pull-in bypass into the EOM because the location of EMO between the suspension and the actuator allows us to directly compare the forces without having extra wire connection; if it were included in the actuator unit, we should have had an extra wire from the suspension unit.

The spring constant k and damping coefficient c have been transferred out to the suspension module, which will be discussed shortly in the next section. As seen in the previous section, the EOM module with cascaded mathematic integration capacitors calculates the velocity and position, and it returns the values to the x and $\dot{x}$ pins on both sides of the subcircuit.

The EOM subcircuit is designed to read in the incoming force as electrical current. This definition allows us to have multiple modules of actuators and suspensions to be parallel-connected into a single EOM module; their force contribution can be simply added by connecting the wires into the receptacle pins of the EOM. Because EDD reads only voltage as input, current-controlled voltage sources ($CCVS_1$–$CCVS_4$) are used at the interface. On the other hand, the EOM module reads out the velocity and displacement in terms of voltage such that they could be delivered to multiple load modules without depression. Voltage-controlled voltage sources ($VCVS_2$–$VCVS_5$) are used as a buffer at the interface.

In our EOM module, we pass displacement and velocity to nearby spring modules by using a constant voltage output, while receiving the reactive force in terms of constant current. The combination of voltage and current has been chosen such that the building block can be jointed not only in a straight chain but also in a branched tree shape. Displacement and velocity imprinted in a constant voltage can be delivered to multiple suspension modules without causing degradation of value, and the reactive force from multiple suspension modules can be added by simply merging wires to the EOM module symbol at the force input pin. A similar convenient benefit can be found when parallel-connecting electrostatic actuator modules to a single EOM.

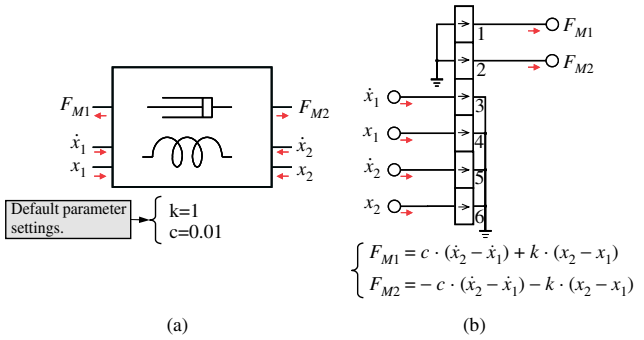

Fig. 6. Equivalent circuit model for viscoelastic suspension: (a) circuit symbol and (b) EDD program. Differential displacement and velocity measured on the two ends $(\dot{x}_1, x_1, \dot{x}_2, x_2)$ are used to calculate reactive restoring force

3.2. Viscoelastic suspension The viscoelastic restoring force has been transferred from the original EOM module (shown in Fig. 4) into an independent subcircuit module. The standardized I/O pins shown in Fig. 6(a) are designed to mate with the EOM module. Spring constant k and damping coefficient c are interpreted by using a combination model for an elastic spring and a dashpot, and it returns the reactive force to the connected EOM module(s) as a function of the velocity and displacement. Considering the direction of the force, the left- and right-hand sides of the module return forces as

$$F_{M1} = c \cdot (\dot{x}_2 - \dot{x}_1) + k \cdot (x_2 - x_1) \tag{13}$$

and

$$F_{M2} = -c \cdot (\dot{x}_2 - \dot{x}_1) - k \cdot (x_2 - x_1) \tag{14}$$

respectively. The suffixes 1 and 2 correspond to the left- and the right-hand sides of the subcircuit module, respectively. The force on the right-hand side of the module (F_{M2}) is designed to 'pull' the connected EOM module toward the $-X$ direction. These forces are implemented in the EDD forms as follows:

$$I_1 \leftarrow c^*(V_5 - V_3) + k^*(V_6 - V_4) \tag{15}$$

and

$$I_2 \leftarrow -c^*(V_5 - V_3) - k^*(V_6 - V_4) \tag{16}$$

where the voltage set of (V_3, V_4, V_5, V_6) is the interpretation for $(\dot{x}_1, x_1, \dot{x}_2, x_2)$, as illustrated in Fig. 6(b). The spring constant k and the damping coefficient c are passed as arguments to the module. In actual MEMS devices, most significant contribution to the damping coefficient may come from the air damping associated with the masses and capacitance plates rather than the springs; in our model, nonetheless, we represent the loss by the dashpod alone for the simplicity. It is also possible to prepare an air-damping model of, for instance, laminar flow [28], and to connect it to the EOM in parallel with the suspension; the detailed modeling is under investigation for future study.

3.3. Electrostatic actuators A subcircuit module for the parallel-plate electrostatic actuator is shown in Fig. 7(a), which is a subset including EDD_1 in the EOM equivalent circuit of Fig. 4. The actuator model is used on the right-hand side of an EOM module, and it pulls the mass toward the $+X$ direction. Accordingly, the force output is defined in the EDD current form as

$$I_1 \leftarrow (1/2)^*\mathrm{ep}_0^*S^*(V_3 - V_2)\hat{}2/(g - V_4)\hat{}2 \tag{17}$$

where (V_2, V_3, V_4) corresponds to (V_A, V_B, x). The dielectric constant parameter $\mathrm{ep}_0 = 8.854 \times 10^{-12}$ F/m is defined in the Qucs

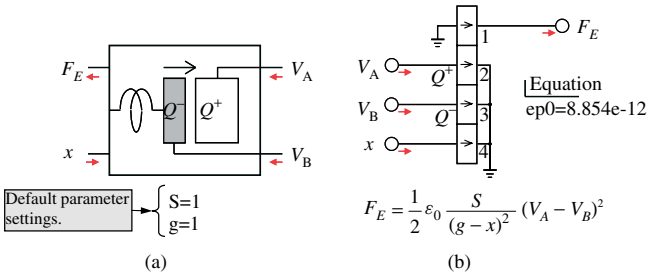

Fig. 7. Equivalent circuit model for parallel-plate electrostatic micro actuator (plate motion toward $+x$): (a) circuit symbol and (b) EDD program. The drive voltages (V_A, V_B) and the plate displacement (x) are read in as voltages (V_2, V_3, V_4), and the output force F_E is represented in a form of current as a function of (V_2, V_3, V_4)

schematic file. The parameters S and g are passed as arguments attached to the subcircuit symbol of the module.

Another interesting feature of EDD is its capability of describing the dielectric charge as a response to the applied voltage; charge induction defines the electrical current flowing into the input port of the EDD block. In Fig. 7(a), Q^+ and Q^- represent the electrical charge induction on the actuator plates, and they are respectively modeled in Fig. 7(b), as

$$Q_2 \leftarrow \mathrm{ep}_0^* S^* (V_2 - V_3)/(g - V_4) \tag{18}$$

and

$$Q_3 \leftarrow \mathrm{ep}_0^* S^* (V_3 - V_2)/(g - V_4) \tag{19}$$

where V_2 and V_3 correspond to V_A and V_B, respectively. By this expression, the electrical equation (4) is automatically included in the electrical circuit model of the EDD with an external resistor R. Another model of parallel-plate actuator that pulls the mass toward the $-X$ direction can also be made in the same manner only by flipping the sign of the displacement V_4. Subcircuit models for other types of mechanisms such as the comb-drive actuator and the electrostatic torsion mirror have been made and they will be reported elsewhere.

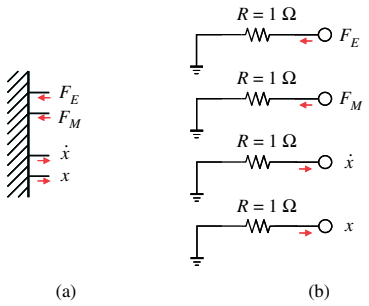

Fig. 8. Equivalent circuit model for mechanical anchor (a and b). Electrical ground level is provided to the suspension module to constrain the displacement and velocity. Resistances are used to dump the restoring force, which is represented in electrical current

3.4. Mechanical anchor For the convenience of applying mechanical constraint to the suspension module, an anchor module has been prepared as shown in Figs. 8(a) and (b). The lower two ports of $\dot{x}$ and x are used to pull down the potential to the ground to provide the $\dot{x} = x = 0$ condition to a connected suspension module. The second port F_M is to terminate the constant current of viscoelastic force flowing from a suspension module. Those 1-Ω resistors used in the anchor module are inserted to avoid the Qucs simulation warnings, and they do not affect the simulation result.

4. Verification of Simulation

4.1. Verification of EOM solver In this section, we investigate the simulation accuracy of the equivalent circuit model by using a verification problem. A coupled oscillator of three bodies of mass m and four springs of rigidity k, as illustrated in Fig. 9(a), is known to have three orthogonal modes at the resonant frequencies $\omega_1 = \sqrt{2 - \sqrt{2}} \cdot \sqrt{k/m}$, $\omega_2 = \sqrt{2} \cdot \sqrt{k/m}$, and

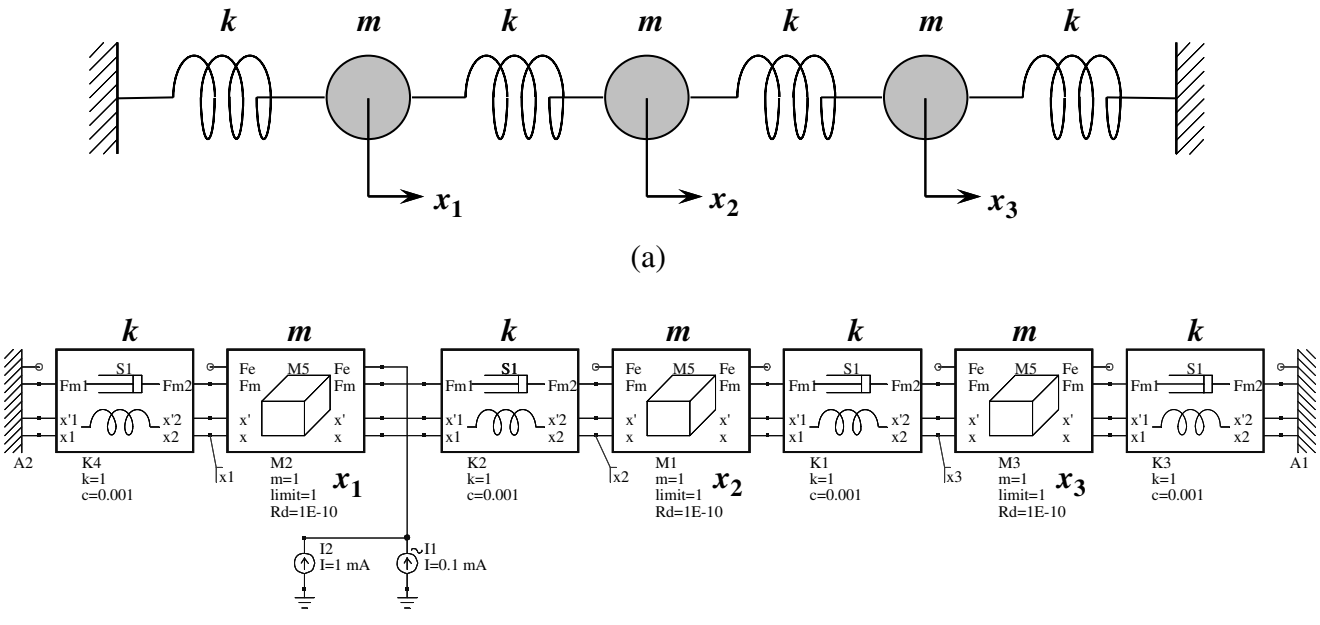

Fig. 9. Equivalent circuit interpretation of three-body coupled oscillators. (a) Schematic model and (b) Qucs representation. The mass on the left-hand side is excited by using the current sources that represent a virtual external force

Table I. Oscillation modes and node amplitudes of three-body coupled oscillators

Mode		Amplitude ratio x_1	x_2	x_3	Resonant angular frequency
1	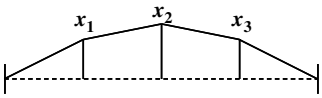	1	$\sqrt{2}$	1	$\omega_1 = \sqrt{2-\sqrt{2}} \cdot \sqrt{\frac{k}{m}} = 0.765\sqrt{\frac{k}{m}}$
		1	1.428	1	0.766
2	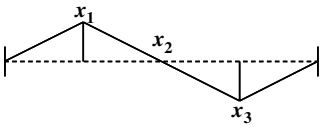	1	0	−1	$\omega_2 = \sqrt{2} \cdot \sqrt{\frac{k}{m}} = 1.414\sqrt{\frac{k}{m}}$
		1	0	−1	1.413
3	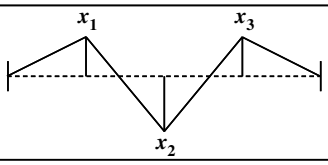	1	$-\sqrt{2}$	1	$\omega_3 = \sqrt{2+\sqrt{2}} \cdot \sqrt{\frac{k}{m}} = 1.848\sqrt{\frac{k}{m}}$
		1	−1.414	1	1.846

$(m, c, k) = (1, 0.001, 1)$

Theoretical analysis results are shown in the upper rows in each mode. Simulation results are in the lower rows.

$\omega_3 = \sqrt{2+\sqrt{2}} \cdot \sqrt{k/m}$. A coupled oscillator for test was built by using the EOM and suspension modules as shown in Fig. 9(b). The first EOM module located on the left-hand side was excited to vibrate by the electrical current sources which represent the external force. The AC simulation function of Qucs was used to plot the frequency response of each EOM module, and the resonant modes and node amplitudes were determined.

Table I summarizes the simulation results; theoretical node amplitudes are shown in the upper rows of each mode, and simulation results are compared in the corresponding lower rows. The parameters were set to be $m = k = 1$ for normalization, and $c = 0.001$ for a large quality factor ($Q = \sqrt{mk}/c = 10^3$) to clearly see the resonant peaks. A total of 360 000 points were linearly sampled in the frequency range between 0.1 and 0.33 Hz, at a sampling density of $\Delta f = 6.3\dot{8} \times 10^{-7}$ Hz. The equivalent circuit model was found to show good agreement with the theoretical results in both mode shapes and node amplitudes. The simulation error was found to be 1% or less, which was good for numerical computation.

4.2. Verification of electrostatic pull-in analysis

Another simulation model for a spring–mass system with a parallel-plate electrostatic actuator has been developed as shown in Fig. 10(a). The subcircuit modules of viscoelastic spring, EOM, and actuator are connected in a chain, and a step-function voltage source was connected to the V_A pin. Dimensional parameters of the actuator are defined in the equation block of Qucs, as listed in Fig. 10(b), which also includes the definition of the theoretical pull-in voltage and resonant frequency. Figure 10(c) specifies the simulation type (transient simulation). A part of the DC level simulation results, such as pull-in voltage and resonant frequency, is shown in Fig. 10(d) for the convenience of programming. Simulation time span is intentionally set to be as long as 2000 ms compared to the natural oscillation period at the resonance, i.e. 0.83 μs, in order to fulfill the quasi-static condition. After the 30-s simulation time on a Windows PC (with Centrino 1.2 GHz and DRAM 1 GB), the obtained displacement curve is presented in the plot diagram Fig. 10(e), along with the drive voltage.

In the solid curve of Fig. 11, we replot the displacement–voltage curve of the simulated parallel-plate actuator. Circles in the same plot are the results of a static simulation model ($kx = \frac{1}{2}\varepsilon_0 \frac{S}{(g-x)^2} V_d^2$) solved by using Newton's method. The initial gap length between the plates is set to be 1 μm, and the stopper is placed at the 0.8-μm position. The pull-in subroutine (EDD_4 in Fig. 5(b)) is activated when the electrical attractive force exceeds the mechanical restoring force, and the routine remains effective until the plate is released at $V_d = 3.8$ V. The developed model clearly exhibited the 1/3-gap criteria of the electrostatic pull-in effect. Damped oscillation is observed at the release edge, thanks to the transient simulation function of Qucs. From this observation, the developed model is thought to reproduce the electromechanical behavior of electrostatic parallel-plate actuator.

4.3. Simulation tolerance

In Section 2.4, we introduced a virtual contact resistance R_d to discharge the integration capacitor C_1 upon mechanical contact (electrostatic pull-in). Due to a technicality of the Qucs simulation algorithm, R_d cannot be zero but a finite small value should be used ($R_d < 10^{-14}$). It is empirically known that an excessively large value of R_d leads to the drift of the contact position.

The output current I_1 from EDD_3, which represents the acceleration in Fig. 5(b), keeps flowing even after the electrostatic pull-in, due to the presence of applied voltage V and the restoring force $k \cdot x_{max}$, as

$$i = \left\{ \frac{1}{2}\varepsilon_0 \frac{S}{(g - x_{max})^2} V^2 - k \cdot x_s \right\} \cdot \frac{1}{m} \tag{20}$$

where x_{max} is the position of the mechanical stopper. The generated current should be dumped to the drain through the pull-in subroutine EDD_4 such that the capacitor C_1 does not build up a voltage signal that corresponds to the velocity. Nevertheless, the EDD_4 has a voltage drop of $R_d \cdot i$ due to the finite value of R_d, and it is passed to the following integration stage as a velocity error. For a finite simulation period of T under the pull-in condition, the error accumulates to cause the drift of displacement by $\Delta x = R_d \cdot i \cdot T$. Presuming an allowable analytical error of $\alpha \cdot x_{max}$, one would obtain

$$R_d \cdot i \cdot T < \alpha \cdot x_{max} \tag{21}$$

Therefore, the condition for R_d is written as

$$R_d < \frac{\alpha \cdot x_{max} \cdot m}{\left\{ \frac{1}{2}\varepsilon_0 \frac{S}{(g - x_{max})^2} V^2 - k \cdot x_{max} \right\} \cdot T} \tag{22}$$

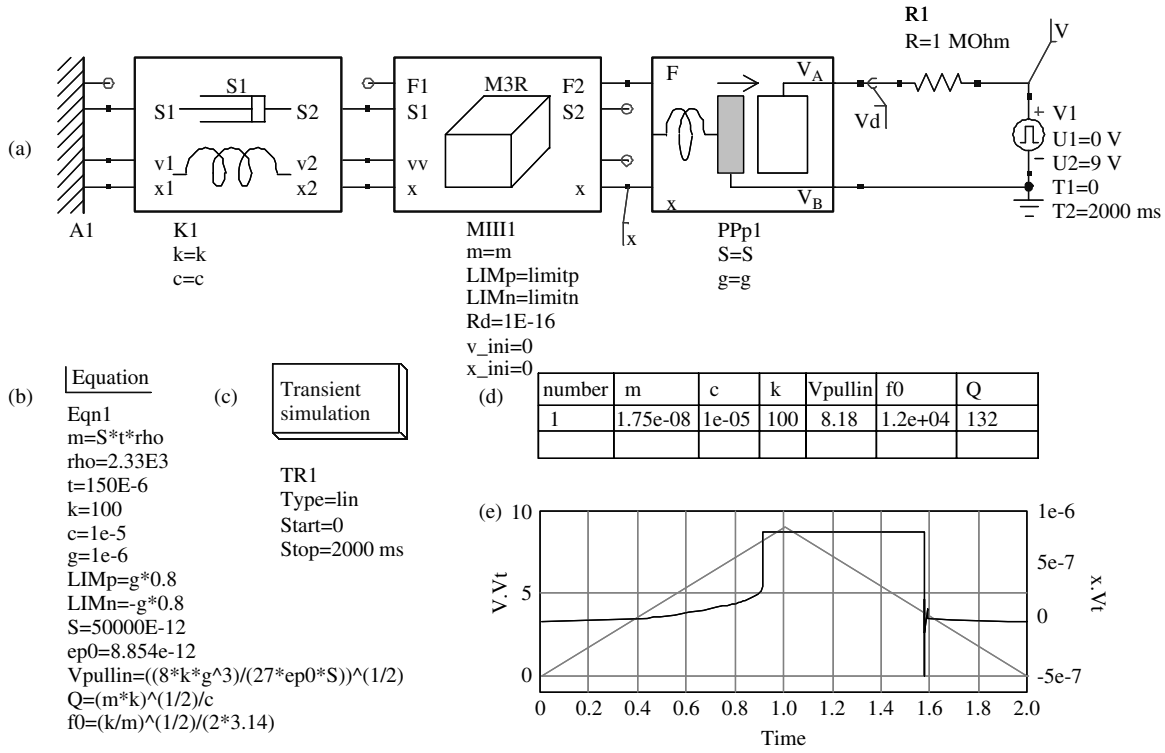

Fig. 10. Qucs simulation screenshot of transient analysis. (a) Simulation model for device under test, (b) parameter configuration, (c) simulation type definition, (d) DC analysis display, and (e) transient analysis results of the plate displacement

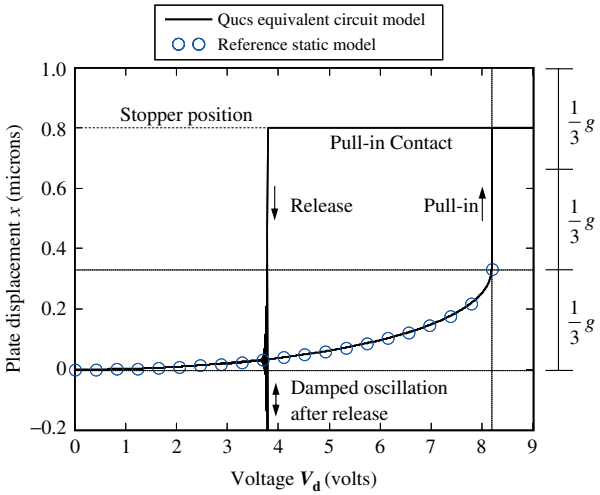

Fig. 11. Transient analysis result of parallel-plate actuator presented in a displacement–voltage form. The rule pull-in behavior of the parallel-plate actuator is reproduced by the simulation

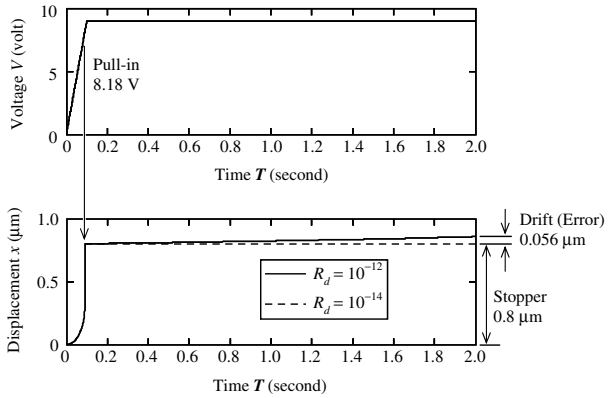

Fig. 12. Influence of parameter R_d on the simulation tolerance for the electrostatic pull-in analysis. The value for the virtual contact resistance R_d should be set as small as 10^{-14} to avoid the accumulation of simulation error

For a practical simulation use, we set $\alpha = 0.001$ (drift error of 0.1%). For the parameters used in Fig. 11, (26) suggests that R_d should be smaller than 1.9×10^{-14}. Figure 12 compares the simulation results calculated with different values of R_d. When $R_d = 10^{-14}$ (dashed curve), calculation error at $T = 2000$ ms was only 0.01 μm, which corresponded to 0.00125 x_{max}; this error is close to the theoretical tolerance of 0.001 x_{max}. When R_d was increased to $R_d = 10^{-12}$ (solid curve), on the other hand, the displacement error increased to 0.056 μm, which was not negligible. Hence R_d should be chosen appropriately according to (22); the value may change depending on the actuator's dimension, operation voltage, and simulation time span.

In other simulation models, displacement limit is implemented in the suspension module by modeling the constant force in an exponential form $F_s \cdot \{\exp(\kappa \cdot x / x_{max}) - 1\}$, where F_s and κ are the fitting parameters to represent the repulsive force magnitude and the contact hardness, respectively [18]. A possible drawback in practical use of this model is that the simulated contact position cannot be exactly made at x_{max} but it is sensitive to the combination of fitting parameters F_s and κ. Our model using EDD, in contrast, guarantees the contact position x_{max} at high accuracy by using only one fitting parameter R_d.

5. Conclusions

We have developed a numerical simulation platform for microelectromechanical actuators and physical sensors by using the open-source electrical circuit simulator Qucs as a platform. Equivalent subcircuit models for the EOM, viscoelastic suspension, and electrostatic actuators have been developed as building blocks for the multiphysics analysis of micromechanism and electronics. Due

to the well-prepared functions of Qucs, various simulation types of MEMS have become possible, including DC analysis, transient analysis, and frequency response analysis. Simulation accuracy has been quantitatively studied by using the already known verification models such as three-body coupled oscillators, parallel-plate electrostatic actuator of pull-in, and negative spring-constant effects.

Qucs is open-source software under the GPL agreement, and it is distributed from the website of the development team [12]. The equivalent circuit models reported in this paper are also subject to the GPL code, and they are posted at the authors' lab homepage for public use [29].

Acknowledgment

We would like to thank Prof. Gen Hashiguchi at the Research Institute of Electronics, Shizuoka University, for technical discussion on MEMS simulation models.

References

(1) Senturia SD. Simulation and design of microsystems: a 10-year perspective. *Sensors and Actuators* 1998; **A67**:1–7.
(2) Gupta RK, Hung ES, Yang Y-J, Ananthasuresh GK, Senturia SD. Pull-in dynamics of electrostatically-actuated beams. *Proceedings of Solid-State Sensor and Actuator Workshop (Hilton Head 1996)*, Late News Session, Hilton Head Island, SC, June 3–6, 1996; 1–2.
(3) Gyimesi M, Avdeev I, Ostergaard D. Finite-element simulation of micro-electromechanical systems (MEMS) by strongly coupled electromechanical transducers. *IEEE Transactions on Magnetics* 2004; **40**(**2**):557–560.
(4) IntelliSense EDA Linker web: http://www.intellisensesoftware.com/ [Last accessed April 2010].
(5) Clark JV, Zhou N, Pister KSJ. Modeling, simulation, and verification of an advanced micromirror using SUGAR. *IEEE Journal of Microelectromechanical Systems* 2007; **16**(**6**):1524–1536.
(6) Lutz M, Partridge A, Gupta P, Buchan N, Klaassen E, McDonald J, Petersen K. MEMS oscillators for high volume commercial applications. *Proceedings of 14th International Conference on Solid-State Sensors, Actuators and Microsystems (Transducers '07)*, Lyon, France, June 10–14, 2007; 49–52.
(7) He L, Xu YP, Palaniapan M. A CMOS readout circuit for SOI resonant accelerometer with 4-μg bias stability and 20-μg/ root Hz resolution. *IEEE Journal of Solid-State Circuits* 2008; **43**(**6**):1480–1490.
(8) Hornbeck LJ. Combining digital optical MEMS, CMOS and algorithms for unique display solutions. *Digest IEEE International Electron Devices Meeting (IEDM 2007),* Washington, DC, USA, December 10–12, 2007; 17–24.
(9) Neumann JJ, Jr, Gabriel KJ. A fully-integrated CMOS-MEMS audio microphone. *Proceedings of 12th International Conference on Solid-State Sensors, Actuators and Microsystems (Transducers 03)*, Boston, USA, June 8–12, 2003; 230–233.
(10) Janus P, Bieniek T, Kociubinski A, Grabiel P, Schropfer G. Modeling and co-simulation of integrated micro and nanosystems. *Proceedings of 14th International Conference on Mixed Design of Integrated Circuits and Systems (MIXDES '07)*, Ciechocinek, Poland, June 21–23, 2007; 439–443.
(11) Basrour S, Matou K, Ammar Y, Marzencki M, Zenati A. Multi-domain and mixed-signal simulation of System-on-Chip embedding MEMS. *Proceedings of 7th International Conference on Thermal, Mechanical and Multiphysics Simulation and Experiments in Micro-Electronics and Micro-Systems (EuroSimE 2006)*, Como, Italy, April 24–26, 2006.
(12) Qucs development team website (multi-platform installation is possible on Windows PC, Unix, Linux, and Mac OS) http://qucs.sourceforge.net/ [Last accessed April 2010].
(13) Mita M, Toshiyoshi H. An equivalent-circuit model for MEMS electrostatic actuator using open-source software Qucs. *IEICE Electronics Express* 2009; **6**(**5**):256–263.
(14) Toshiyoshi H. Electrostatic actuation. In *Comprehensive Microsystems*, vol. 2. Gianchandani YB, Tabata O, Zappe H (eds). Elsevier: Amsterdam, 2008; 1–38.
(15) Grigorie TL. The Matlab/Simulink modeling and numerical simulation of an analogue capacitive micro-accelerometer. Part 1: open loop. *Proceedings of 4th International Conference on Perspective Technologies & Methods in MEMS Design* (*MEMSTECH* 2008), Lviv, Ukraine, 2008; 105–114.
(16) PLECS—a toolbox for Matlab/Simulink http://www.plexim.com/ [Last accessed April 2010].
(17) Howe RM. Fundamentals of the analog computer circuits: technology, and simulation. *IEEE Control System Magazine* 2005; **25**(**3**): 29–36.
(18) Veijola T. Nonlinear circuit simulation of MEMS components: controlled current source approach. *Proceedings of ECCTD'01*, Espoo, Finland, August 28–31, vol. 3, 2001; 377–380.
(19) Takahashi T, Maruyama S, Mita M, Fujita H, Toshiyoshi H. A mixed-signal analysis tool for MOEMS based on circuit simulator. *Proceedings of IEEE Optical MEMS and Nanophotonics 2009*, Clearwater Beach, Florida, USA, August 17–20 2009, ThB1.
(20) Moseley SH, Arendt R, Boucarut RA, Jhabvala M, King T, Kletetschka G, Kutyrev AS, Li M, Meyer S, Rapchun D, Silverberg RF. Microshutters arrays for the JWST near infrared spectrograph. *Proceedings of SPIE* 2004; **5487**(**1**):645–652.
(21) Toshiyoshi H, Kobayashi D, Mita M, Hashiguchi G, Fujita H, Endo J, Wada Y. Microelectromechanical digital-to-analog converters of displacement for step motion actuators. *IEEE Journal of Microelectromechanical Systems* 2000; **9**(**2**):218–225.
(22) Mita M, Toshiyoshi H, Ataka M, Fujita H. A Micro Dice: an electrostatic micro random number generator. *Proceedings of 18th IEEE International Conference on Micro Electro Mechanical Systems (MEMS* 2005), Miami Beach, Florida, USA, January 30–February 3, 2005.
(23) Mita M, Ataka M, Ishida T, Fujita H, Toshiyoshi H. Frequency transition phenomenon of self-oscillated micro cantilever by changing driving voltage. *Proceedings of 14th International Conference on Solid-State Sensors, Actuators and Microsystems (Transducers '07)*, Lyon, France, June 10–14, 2007.
(24) Mukherjee T, Fedder GK. Hierarchical mixed-domain circuit simulation, synthesis and extraction methodology for MEMS. *Journal of VLSI Signal Processing* 1999; **21**:233–249.
(25) Nishimori Y, Ooiso H, Mochizuki S, Fujiwara N, Tsuchiya T, Hashiguchi G. A multiple degree of freedom equivalent circuit for a comb-drive actuator. *Japanese Journal of Applied Physics* 2009; **48**:124504.
(26) Wen F, Li W, Huang Q-A, Rong H. Large-signal lumped-parameter macromodels for the equivalent circuit representation of electromechanical transducers. *Journal of Micromechanics Microengineering* 2004; **14**:452–461.
(27) Beznosyk O, Finogenov O, Ladogubets V, Tchkalov O. Using circuit design software to simulate mechanical components. *Proceedings of MEMSTECH'2008*, Polyana, Ukraine, May 21–24, 2008; 130–133.
(28) Cho Y-H, Kwak BM, Pisano AP, Howe RT. Viscous energy dissipation in laterally oscillating planar microstructures: a theoretical and experimental study. *Proceedings of IEEE Micro Electro Mechanical Systems (MEMS'93)*, Fort Lauderdale, FL, USA, February 7–10, 1993; 93–98.
(29) Equivalent circuit models are distributed at the author's lab home page at http://toshi.iis.u-tokyo.ac.jp/toshilab/ [Last accessed April 2010].

Makoto Mita (Member) received the B.E. degree from Tohoku University, Sendai, Japan, and the M.E. and Ph.D. degrees in 1999 and 2002, respectively, from The University of Tokyo, Tokyo, Japan. Since 2003, he has been an Assistant Professor with the Institute of Space and Astronautical Science, Japan Aerospace Exploration Agency, Kanagawa, Japan. He is also currently with the Institute of Industrial Science, The University of Tokyo. His research interests include MEMS for space applications and nanomechatronics.

Satoshi Maruyama (Student Member) received B.S. degree in electronic and electrical engineering from Gunma University, Maebashi, Japan, in 2008. He is currently working toward the M.S. degree at the Institute of Industrial Science, The University of Tokyo, Tokyo, Japan. His research interests include the development of multiphysics simulation models for MEMS and LSI.

Yuheon Yi (Non-member) received the B.S. degree in electronic and electrical engineering from Pohang University of Science and Technology, Pohang, Korea, in 1999, the M.S. degree in biosystems from the Korea Advanced Institute of Science and Technology, Daejeon, Korea, in 2004, and the Ph.D. degree in electrical engineering from The University of Tokyo, Tokyo, Japan, in 2009, where he developed the design and fabrication technologies for integrated MEMS. Since 2009, he has been a Research Assistant with Research Center for Advanced Science and Technology (RCAST), The University of Tokyo. His research interests also include the development of behavioral models for MEMS actuators and sensors.

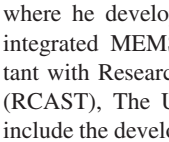

Kazuhiro Takahashi (Member) received the B.S. degree in mechanical engineering from Nagoya University, Nagoya, Japan, in 2003, and the M.S. and Ph.D. degrees in electrical engineering from The University of Tokyo, Tokyo, Japan, in 2005 and 2008, respectively. He is currently an Assistant Professor with Toyohashi Institute of Technology, Toyohashi, Japan. His research interest includes integration technologies between MEMS actuators and CMOS control circuits for optical and bio MEMS applications.

Hiroyuki Fujita (Member) received the B.S., M.S., and Ph.D. degrees in electrical engineering from The University of Tokyo, Tokyo, Japan, in 1975, 1977, and 1980, respectively. He has been with the Institute of Industrial Science, The University of Tokyo, where he was a Lecturer in 1980–1981, an Associate Professor from 1981 to 1993, and a Professor since 1993. He has also been the Director of the Center for International Research on MicroMechatronics, Institute of Industrial Science, The University of Tokyo, since 2003. He is currently engaged in the investigation of microelectromechanical systems fabricated by IC-based processes and applications to optics, hard-disk drives, and biotechnology/nanotechnology. He is also interested in autonomous distributed microsystems.

Hiroshi Toshiyoshi (Member) received the M.E. and Ph.D. degrees in electrical engineering from The University of Tokyo, Tokyo, Japan, in 1993 and 1996, respectively. Since 2002, he has been an Assistant Professor with the Institute of Industrial Science, The University of Tokyo. From 1999 to 2001, he was a Visiting Assistant Professor at the University of California Los Angeles. From 2002 to 2007, he was a codirector of LIMMS/CNRS-IIS UMI-2820, an international joint lab with CNRS France. From 2005 to 2008, he has been a project leader of the Optomechatronics Project at Kanagawa Academy of Science & Technology (KAST). Since May 2009, he has been a Professor with Research Center for Advanced Science and Technology (RCAST) attached to The University of Tokyo. His research interests include optical and RF-MEMS.